NAVAL

POSTGRADUATE

SCHOOL

MONTEREY, CALIFORNIA

THESIS

DEMONSTRATION OF A NEAR AND MID-INFRARED DETECTOR USING MULTIPLE STEP QUANTUM WELLS

by

Michael P. Touse

September 2003

Thesis Advisor:	Gamani Karunasiri
Second Reader:	James Luscombe

Approved for public release; distribution is unlimited.

THIS PAGE INTENTIONALLY LEFT BLANK

REPORT DOCUMENTATION PAGE

Public reporting burden for this collection of information is estimated to average 1 hour per response, including the time for reviewing instruction, searching existing data sources, gathering and maintaining the data needed, and completing and reviewing the collection of information. Send comments regarding this burden estimate or any other aspect of this collection of information, including suggestions for reducing this burden, to Washington headquarters Services, Directorate for Information Operations and Reports, 1215 Jefferson Davis Highway, Suite 1204, Arlington, VA 22202-4302, and to the Office of Management and Budget, Paperwork Reduction Project (0704-0188) Washington DC 20503.

1. AGENCY USE ONLY *(Leave blank)*	2. REPORT DATE September 2003	3. REPORT TYPE AND DATES COVERED Master's Thesis

4. TITLE AND SUBTITLE Demonstration of a Near and Mid-Infrared Detector Using Multiple Step Quantum Wells	5. FUNDING NUMBERS
6. AUTHOR (S) Michael P. Touse	

7. PERFORMING ORGANIZATION NAME(S) AND ADDRESS(ES) Naval Postgraduate School Monterey, CA 93943-5000	8. PERFORMING ORGANIZATION REPORT NUMBER

9. SPONSORING / MONITORING AGENCY NAME(S) AND ADDRESS(ES) N/A	10. SPONSORING/MONITORING AGENCY REPORT NUMBER

11. SUPPLEMENTARY NOTES The views expressed in this thesis are those of the author and do not reflect the official policy or position of the U.S. Department of Defense or the U.S. Government.

12a. DISTRIBUTION / AVAILABILITY STATEMENT Approved for public release; distribution is unlimited	12b. DISTRIBUTION CODE

13. ABSTRACT *(maximum 200 words)*

In this thesis a device was designed to ultimately detect a laser designator operating at 1.06 μm and infrared radiation near 10 μm simultaneously. The final design consisted of 25 quantum step wells 80 μm wide. The peak IR absorption coefficient was 1800 cm^{-1} at 11.1 μm with a bandwidth of 1.6 μm. Dark current was measured to be 1.6 x 10^{-8} A at 1 V bias at 10 K and a background photocurrent of 4.6 x 10^{-6} A at 10 K. The background-limited performance of the device occurs at approximately 55 K. The barrier height of the well was 99 meV. The maximum responsivity for each band was measured to be 0.04 A/W at 840 nm and 0.69 A/W at 10.93 μm.

Detectivity was then calculated to be 3.4 x 10^{10} cm$\sqrt{\text{Hz}}/W$ in the NIR band and 6.5 x 10^{11} cm$\sqrt{\text{Hz}}/W$ in the IR band. D* at the background limited point (D*$_{\text{BLIP}}$) was 2.0 x 10^{9} cm$\sqrt{\text{Hz}}/W$ in the NIR and 3.9 x 10^{10} cm$\sqrt{\text{Hz}}/W$ in the IR.

14. SUBJECT TERMS Quantum Well Infrared Photodetector; QWIP; FTIR;	15. NUMBER OF PAGES 77
	16. PRICE CODE

17. SECURITY CLASSIFICATION OF REPORT Unclassified	18. SECURITY CLASSIFICATION OF THIS PAGE Unclassified	19. SECURITY CLASSIFICATION OF ABSTRACT Unclassified	20. LIMITATION OF ABSTRACT UL

i

THIS PAGE INTENTIONALLY LEFT BLANK

DEMONSTRATION OF A NEAR AND MID-INFRARED QUANTUM WELL INFRARED DETECTOR

Michael P. Touse
Lieutenant, United States Navy
B.S. Physics, United States Naval Academy, 1997

Submitted in partial fulfillment of the
requirements for the degree of

MASTER OF SCIENCE IN PHYSICS

from the

NAVAL POSTGRADUATE SCHOOL
September 2003

Author: Michael P. Touse

Approved by: Gamani Karunasiri
                 Thesis Advisor

                 James Luscombe
                 Co-Advisor

                 James Luscombe
                 Chairman, Department of Physics

iii

THIS PAGE INTENTIONALLY LEFT BLANK

ABSTRACT

In this thesis a device was designed to ultimately detect a laser designator operating at 1.06 μm and infrared radiation near 10 μm simultaneously. The final design consisted of 25 quantum step wells 80 μm wide. The peak IR absorption coefficient was 1800 cm^{-1} at 11.1 μm with a bandwidth of 1.6 μm. Dark current was measured to be 1.6 x 10^{-8} A at 1 V bias at 10 K and a background photocurrent of 4.6 x 10^{-6} A at 10 K. The background-limited performance of the device occurs at approximately 55 K. The barrier height of the well was 99 meV. The maximum responsivity for each band was measured to be 0.04 A/W at 840 nm and 0.69 A/W at 10.93 μm. Detectivity was then calculated to be 3.4 x 10^{10} cm$\sqrt{Hz}/W$ in the NIR band and 6.5 x 10^{11} cm$\sqrt{Hz}/W$ in the IR band. D* at the background limited point (D*$_{BLIP}$) was 2.0 x 10^{9} cm$\sqrt{Hz}/W$ in the NIR and 3.9 x 10^{10} cm$\sqrt{Hz}/W$ in the IR.

THIS PAGE INTENTIONALLY LEFT BLANK

TABLE OF CONTENTS

THIS PAGE INTENTIONALLY LEFT BLANK

LIST OF FIGURES

THIS PAGE INTENTIONALLY LEFT BLANK

LIST OF TABLES

THIS PAGE INTENTIONALLY LEFT BLANK

ACKNOWLEDGEMENTS

I would like to thank Professor Gamani Karunasiri for the tremendous amount of time and effort he devotes to teaching all of his students. His knowledge and intuition was invaluable throughout the course of this research and working under his supervision is an experience I will always treasure.

Second, I must thank all of the Physics Department faculty and staff. Together they have developed a fantastic program through which I have learned more than I ever thought possible.

Finally, I cannot thank my family enough. To my parents, thank you for teaching me to never stop learning; and to my wife and best friend, thank you for always being by my side and for making it such a joy to come home everyday.

THIS PAGE INTENTIONALLY LEFT BLANK

I.   INTRODUCTION

A.   QUANTUM WELL INFRARED PHOTODETECTORS (QWIP)

Detecting infrared (IR) radiation is a critical technology that has grown rapidly throughout the last thirty years.   It is used in the fields of medicine, astronomy, chemistry, manufacturing, remote sensing, and many others.   Professionals in each of these fields continue to search for improved detectors for their individual applications and have achieved remarkable results in both performance and cost improvements.

Conduction band

E_p

E_g
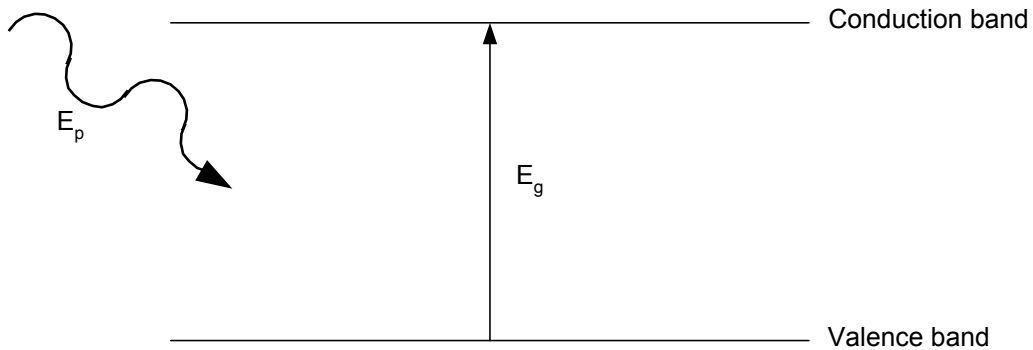
Valence band

Figure 1.   Diagram of valence and conduction band in a semiconductor showing an incoming photon.   The photon energy must be greater than the bandgap for absorption to occur.

Light detectors for use in digital applications are generally created by matching the gap between a material's valence and conduction bands (called a bandgap, E_g) to the photon energy (E_p) of the light one wishes to detect.   An electron in the valence band of the material absorbs all of the photon's energy and is excited into the conduction band of the material as schematically shown in Figure 1.

1

Multiple electrons excited into the conduction band create voltages or currents that can be processed by semiconductor devices according to the application.

This type of detector presents several problems. One problem is that it is very difficult to find materials with certain bandgaps, namely, those less than that of silicon (1.12 eV). Once a material is chosen, detection is limited to a selected band of wavelengths. Common materials used for detection of light in the 1-10 micron range are mercury cadmium telluride (HgCdTe or MCT), indium antimonide (InSb), and platinum silicide (PtSi).
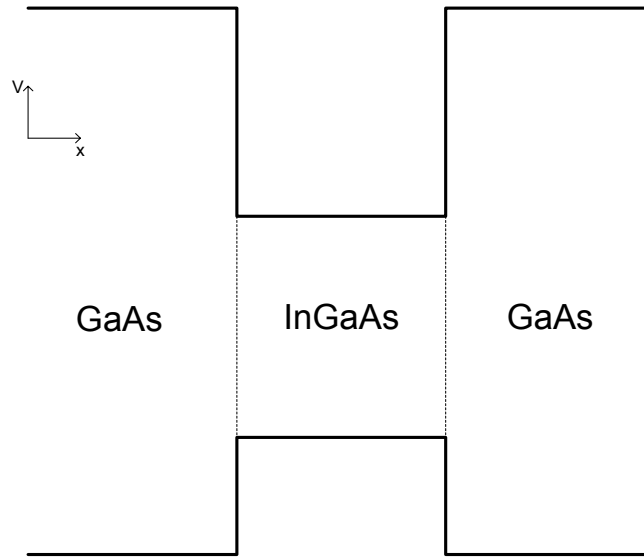
Figure 2. Drawing of potential versus position in InGaAs when the percentage of indium is changed between zero and a non-zero constant.

Quantum Well Infrared Photodetectors (QWIPs) overcome many of the problems of traditional devices because a single material can be fabricated to achieve detection at a wide range of wavelengths. By layering two different

materials, one can create regions of two different bandgaps. For example, separating two regions of GaAs by a region of InGaAs creates a square potential well as shown in Figure 2. By varying the amount of indium in InGaAs, one can change the depth of the potential well and basic quantum mechanics predicts the absorption of a particular frequency within the well. Absorption that takes place between energy levels entirely contained in the conduction band, as seen in Figure 3 is classified as intersubband absorption. Absorption that occurs between the valence and conduction band is considered interband or band-to-band absorption.
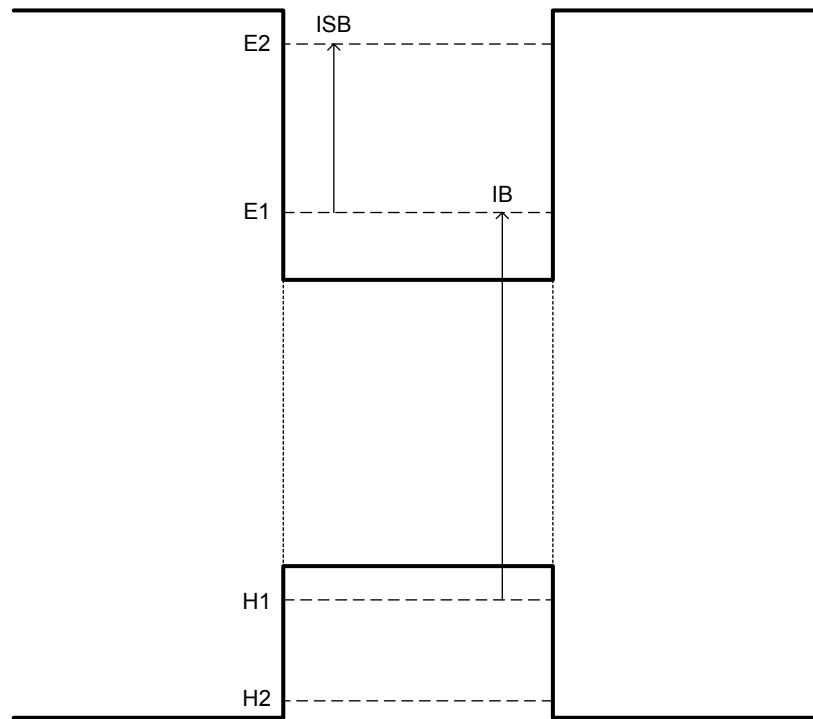
Figure 3.   Drawing of intersubband (ISB) and interband (IB) transitions in a square quantum well.

3

QWIPs can be easily created for a wide range of wavelengths from near-infrared (NIR) to long-wave infrared (LWIR), and can even be tuned near the designed wavelength. They are relatively easy to manufacture using existing semiconductor growth technology, namely, molecular beam epitaxy (MBE). One of the advantages of QWIPs is the ability for a single device to detect multiple colors.

B.   PURPOSE OF THIS THESIS

The purpose of this thesis is to design and evaluate the performance of a two-color asymmetric quantum well infrared photodetector. It uses a design aid created for an earlier thesis (Lantz, 2002) to select the structure needed to achieve absorption of wavelengths near one micron as well as wavelengths between eight and ten microns using both interband and intersubband absorption.

After fabricating the device it will be analyzed using several different characterization methods. Fourier-transform infrared spectroscopy will be used to examine absorption. Current versus voltage will be determined using a semiconductor analyzer. Photoresponse will be measured using a characterization system designed in a previous thesis (Herdlick, 2002).

C.   MILITARY RELEVANCE

The current vision for the technology being pursued in this thesis lies with laser-guided weapons. Laser designators used on military aircraft such as the F-18 use lasers with a wavelength of 1.06 μm (Lantz, 2002, p.5). Often an infrared imaging device (near 10 μm) must also be

used to see the target during nighttime missions. When using different platforms for target designation and weapons delivery, an additional wing pod must be installed which limits the number of other sensors the aircraft can carry. By combining detection of NIR and IR light into a single device, the two systems could be combined into one and allow the valuable space for another sensor. Combining the systems would also greatly reduce the calibration errors associated with combining signals from multiple systems onto a single display.

THIS PAGE INTENTIONALLY LEFT BLANK

II. QWIP BACKGROUND

A. THEORY

As discussed in the introduction, in order for a photon to be absorbed and an electron to be excited, the photon energy must be greater than the energy separation between the valence and conduction bands. To use a material to detect a particular wavelength of light, the bandgap of the material must satisfy (Kasap, 2002, p. 259)

$$E_g < \frac{hc}{\lambda} .$$ (2.1)

Once the material is chosen it acts as a low-pass filter, transmitting all photon energies less than E_g. In order to detect longer wavelengths (lower energies) there must be an available state to which electrons or holes can transition so the photons can be absorbed. Bulk materials have no such states in the gap, giving rise to a single cutoff at the bandgap.

A solution to the lack of allowed electron transitions comes from the ability to fabricate potential wells using semiconductor heterostructures. A common exercise in basic quantum mechanics is to solve Schrödinger's wave equation for a one-dimensional square potential well as shown in Figure 4. When boundary conditions are considered, this yields several discrete energy levels inside the well (Griffiths, 1995).
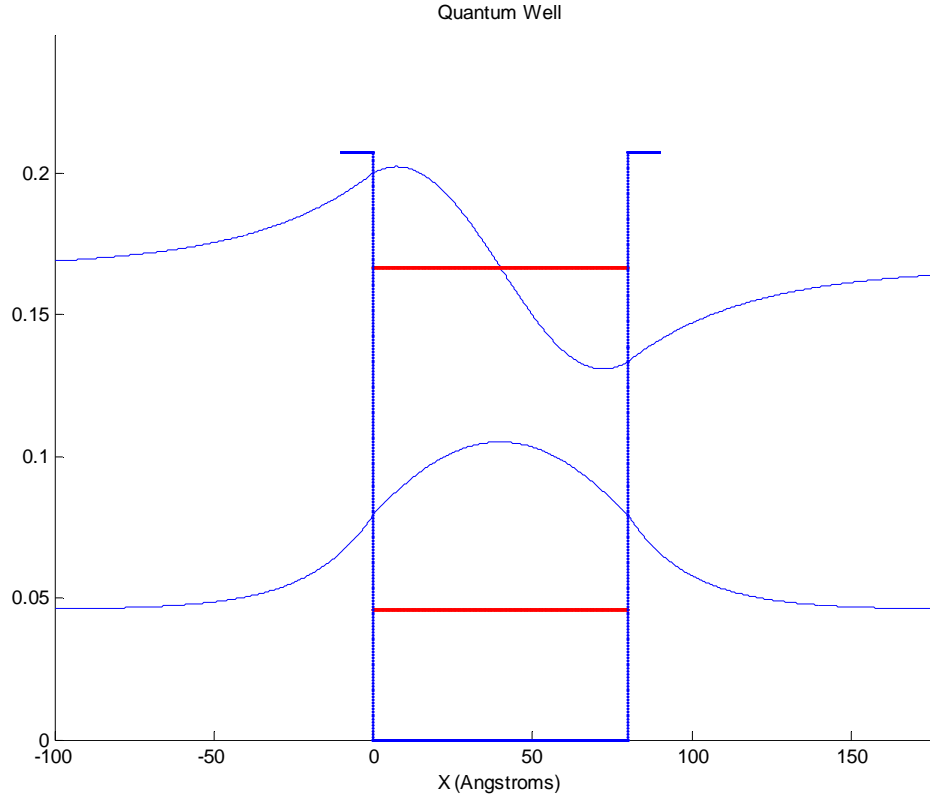
Figure 4.   Drawing of a square potential well
   showing two discrete energy levels with wave
   functions superimposed.   Units are arbitrary.

These discrete energy levels can now be used for IR detection assuming two energy levels can be created with an energy separation approximately equal to the energy of the incoming photons to be absorbed.   Further calculation, however, reveals that certain transitions are forbidden, particularly the interband transition from an odd state to an even state in a symmetric potential well.

Since the transition rate of electrons from energy state E_I to E_F is given by

$$W = \frac{2\pi}{\hbar} \sum_F \left| \left\langle \psi_F \left| V_P \right| \psi_I \right\rangle \right|^2 \delta \left(E_F - E_I - \hbar\omega \right) \qquad (2.2)$$

where (Coon *et al.*, 1984)

$$V_P = \frac{e}{m^*} \left(\frac{I\hbar}{2\varepsilon_0 \varepsilon \omega c} \right)^{\frac{1}{2}} \hat{\boldsymbol{\varepsilon}} \cdot \mathbf{p}_e \qquad (2.3)$$

is the interaction potential. $\hat{\boldsymbol{\varepsilon}}$ is the polarization of the incident photon and $\mathbf{p}_e$ is the momentum of the electron given by

$$\mathbf{p}_e = \frac{\hbar}{i} \nabla . \qquad (2.4)$$

The wave function can be written as

$$\psi_s = u_{cell} \phi_s \qquad (2.5)$$

in which s denotes the initial or final state of the electron in the potential well and u_{cell} is the cell periodic function in the material. ϕ_s is the envelope function of the particular state and varies slowly over one crystal cell. Finally, the matrix elements given in the transition rate (Eq 2.2) can be consolidated as

$$\boxed{ \left\langle \psi_F \left| V_P \right| \psi_I \right\rangle \approx \left\langle u'_{cell} \left| \hat{\boldsymbol{\varepsilon}} \cdot \mathbf{p}_e e^{i\mathbf{s} \cdot \mathbf{p}} \right| u_{cell} \right\rangle \left\langle \phi_F \middle| \phi_I \right\rangle + \left\langle u'_{cell} \middle| u_{cell} \right\rangle \left\langle \phi_F \left| \hat{\boldsymbol{\varepsilon}} \cdot \mathbf{p}_e e^{i\mathbf{s} \cdot \mathbf{p}} \right| \phi_I \right\rangle }. \quad (2.6)$$

The bra-ket containing the interaction potential in each term determines the transition strength of the interaction and the bra-ket without the interaction potential determines the selection rules. It is also important to notice that the inner product of the polarization with the momentum of the incoming photon goes

to zero if the photon polarization and electron momentum are perpendicular to each other. This is particularly important for intersubband transitions where the strength is determined by the second term of equation 2.6. Since the envelope function depends only on the x-coordinate (growth direction) an incident photon must have a component of polarization in the x direction to contribute to absorption. This fact will be used in Chapter IV to explain the polarization dependence of absorption.

In an interband (band-to-band) transition involving quantum wells, the second term always goes to zero because the cell periodic functions in the two bands are orthogonal. In a symmetric potential well the first term also goes to zero between odd and even states because the envelope functions are orthogonal to each other (Figure 4). Therefore, in a symmetric well, interband transitions from odd to even states (or vice-versa) are forbidden.

B. DESIGN OF A TWO-COLOR DETECTOR
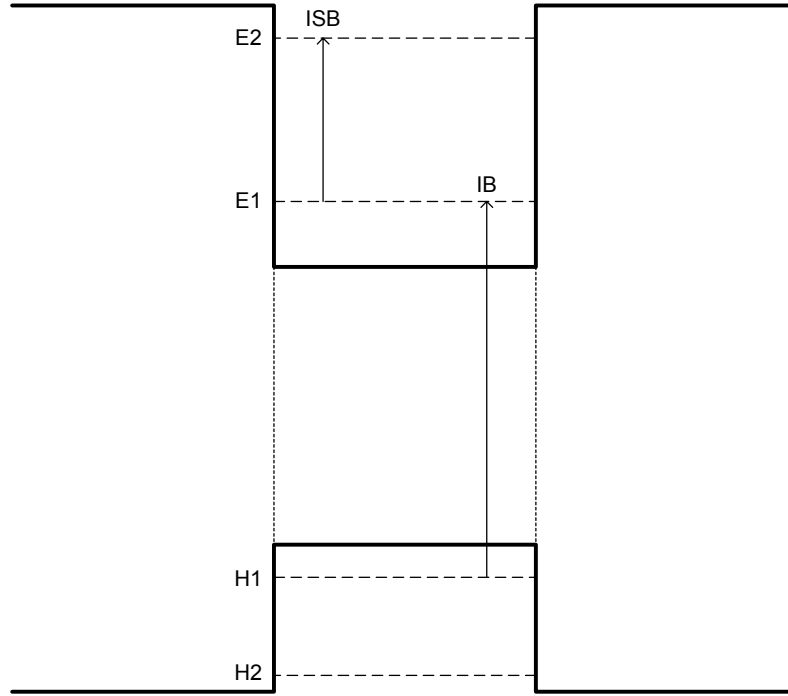
Figure 5. Drawing   of   interband   (IB)   and
intersubband (ISB) transitions in a square
quantum well.

In   the   design   of   the   two-color   detector   it   is
important to take into account the allowed transitions in
the quantum well.   Figure 5 shows the potential well is
created in both the valence and conduction bands of a
semiconductor based quantum well.   In III-V based quantum
wells the well is normally deeper in the conduction band
than in the valence band. For the detector to operate
efficiently it is necessary to have the excited electron
state (E2) close to the top of the barrier.   In the case of
the square potential well, the transition H1 to E2 is not
allowed.   The allowed transition H1 to E1 is not suitable

since the excited electron has to climb a barrier to escape from the well. This suggests that a symmetric quantum well is not suitable for the fabrication of a two-color detector.
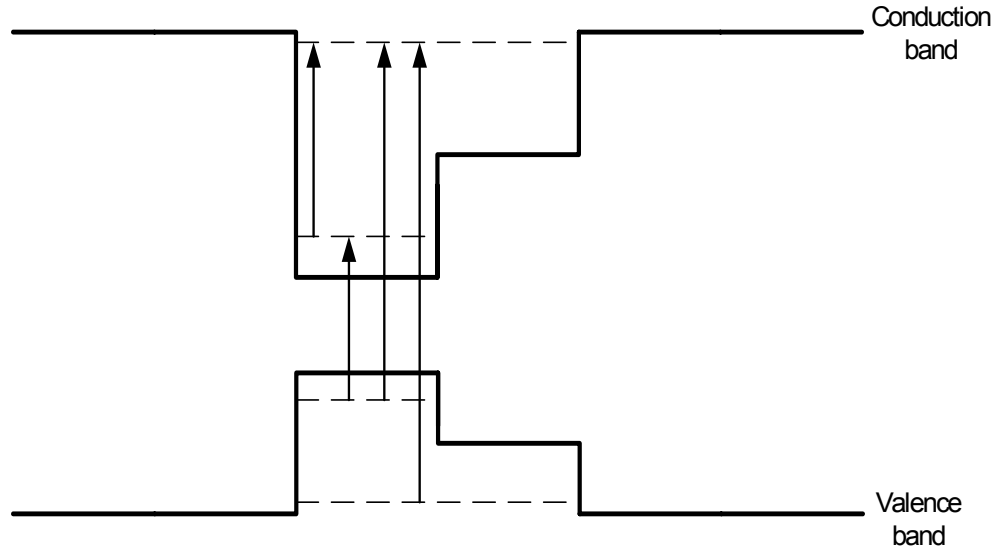
Figure 6.   Drawing   of   potential   step   well showing allowed transitions.

However, if the well is not symmetric as in Figure 6, the two wave functions are not necessarily orthogonal and the transition from an odd to an even state would be possible. By breaking the symmetry of the well, the odd-even transition could be allowed and used for absorption (Mii, *et al.,* 1990). One way to do this is to place two wells of different sizes next to each other causing a step potential as in Figure 6. Another way to achieve this is to apply a relatively large bias across the square potential well causing a slant to the well. Large biases can be problematic during practical use due to excessive noise caused by larger currents (Schneider, *et al.,* 1996). The device used for this thesis is a step quantum well

12

using the transition from H1 to E2 through E_g for the NIR absorption and E1 to E2 for the IR absorption. In order to achieve intersubband transitions, the quantum well must be doped to populate the ground state, E1.

Once a device is designed which contains electron and hole energy levels appropriate for the application, the electrons must be forced to transition to the desired state. This can be done by absorbing photons of the appropriate energy. In addition, the electrons in the E1 state can be excited by thermionic emission. The number of electrons in an excited energy state is approximated by the Boltzmann distribution given in terms of the Fermi energy, E_F, Boltzmann's constant, k_B, and the absolute temperature, T, as (Kasap, 2002, p.286)

$$f(E) = \exp\left[\frac{-(E - E_F)}{k_B T}\right].$$ (2.7)

Since the thermionic emission increases exponentially with temperature, at some point the number of electrons in an excited state due to thermionic emission will far exceed the number there due to incident light. The device must, therefore, be cooled to avoid a situation where the thermal leakage current completely masks the photocurrent.

To make a device employable, the excited electrons must either create an electric potential between the two sides of the device or create a current when an electric potential is applied. In the device for this thesis the latter method is used since the excited electrons do not exist long enough without bias to sustain an internal electric field. Using bias creates a potential gradient

13

across the device and electrons excited to a level near the top of the potential well can travel out of the well and follow the electric field or they can tunnel through the narrowed barrier (Figure 7). Interband transitions to lower energy states (for example, H1 to E1) contribute to absorption, but do not contribute to photocurrent because the excited electrons cannot be removed from the well. It should also be noted that light with wavelengths less than 0.84 μm will not transmit through the substrate and will not reach the active region of the detector if incident from the backside. This will limit the short wavelength response of the detector for backside illumination.
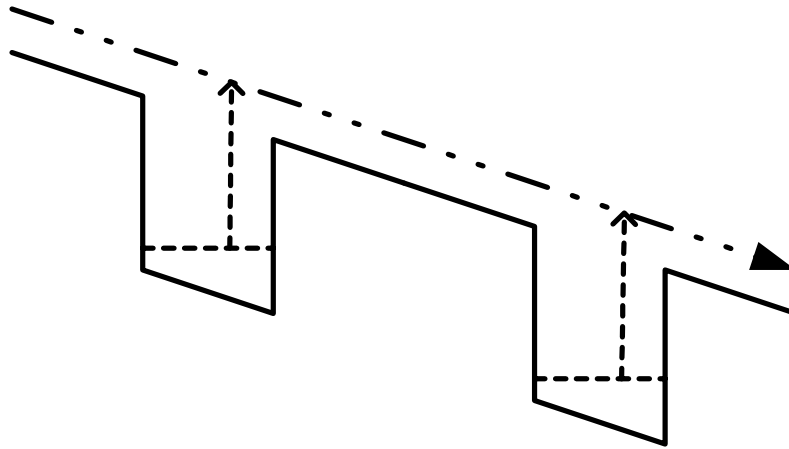
Figure 7. Drawing of multiple square wells under an external bias. Electrons are excited from the well to the continuum above the well and contribute to the photocurrent.

A physical one-dimensional potential well can easily be grown using modern semiconductor growth techniques. Molecular beam epitaxy (MBE) is preferred for QWIPs because it uses less heat than other processes (such as Metal Oxide

Chemical Vapor Deposition, MOCVD) and causes fewer dislocations, in particular for strained layer epitaxy. A semiconductor crystal can be grown and other materials can be combined with the base material to create several layers, each with a different bandgap. For the step quantum well GaAs is used and indium is combined with it in specific percentages. The layer with the highest percentage of In will form the base of the well and layer with no In will form the barrier between wells as shown previously in Figure 2.

THIS PAGE INTENTIONALLY LEFT BLANK

III. DESIGN OF SAMPLES

A.   INITIAL ASSUMPTIONS

The device designed in this thesis should meet two requirements. It must detect a spot from laser designators currently used for laser-guided munitions and detect thermal images in the long-wave infrared region.

As stated in the introduction, current military systems use laser designators operating at 1.06 μm and sets the first requirement, but the second requirement remains somewhat flexible depending upon the temperatures (wavelengths) to be imaged. The maximum intensity of light emitted from a blackbody at a given temperature has a particular wavelength given by Wien's Displacement Law (Dereniak *et al.*, 1996, p. 70):

$$\lambda\max = \frac{2898(\mu m \cdot K)}{T(K)}. \qquad (3.1)$$

Therefore a central wavelength of 10 microns is selected for thermal imaging, which (assuming a 1 μm bandwidth) corresponds to approximate temperatures of $3°C$–$32°C$ ($37°F$–$90°F$).

In order to design an efficient photodetector, the strain induced by lattice mismatch must be minimized when dealing with heterostructures made of lattice-mismatched semiconductors. Because InAs and GaAs have a relatively large variation in lattice parameters (.61 nm and .57 nm, respectively)(Kasap, 2002), the amount of In used in the $Ga_xIn_{1-x}As$ device must be balanced to reduce the lattice mismatch (large x) and maintain sufficient bandgap (small

x). A value of 0.7 was chosen as the largest value of x and a width of 4 nm was used for the lowest portion of the step well. A larger value was then chosen for the step portion of the well to minimize the overall lattice mismatch.

A further constraint requires the upper energy level of the intersubband transition to be very near the maximum potential of the surrounding barrier. This enables the electrons to be ejected from the well and help induce adequate current for detection.

B.   MATLAB ANALYSIS

The remainder of the design was accomplished through the use of a Matlab program developed by Kevin Lantz (2002). This program uses a transfer matrix method to solve the Schrödinger equation for the step quantum well.

Given the proper inputs, the program draws the conduction band structure of the quantum well and computes the energy levels obtained from solving Schrödinger's equation. Required inputs include molar fraction of Ga and In in each step of the well and the width of each step. From this output solution, the absorption spectrum is then computed and plotted.

The device actually produced for this thesis differs from that proposed by Lantz to demonstrate the feasibility of such a device in a cost effective manner. Production of the quarternary material to match the Lantz' proposed device would be too expensive at this early stage, but remains a viable design for future work.

18

	Substance	Mole %	Thickness (A)	Si Doping Concentration (cm^-3)
	GaAs		5000	1E+18
	GaAs		300	
25x	InGaAs	10	40	
	InGaAs	30	40	1E+18
	GaAs		500	
	GaAs		8000	1E+18
	GaAs		6.35E+06	

Table 1 Wafer specifications as provided by manufacturer, IQE Inc.

After several iterations of parameters, the optimum design consisted of 25 step quantum wells with 40 $\overset{\circ}{A}$ wide well and 40 $\overset{\circ}{A}$ wide step. A 300 $\overset{\circ}{A}$ barrier between wells is used as shown in Table 1 and Figure 8 to reduce tunneling between wells. The design predicted an IR absorption peak at 10.2 μm with a cutoff at approximately 12 μm.

500 nm — GaAs

30 nm — Undoped GaAs Barrier

4 nm — In(.1)Ga(.9)As

4 nm — 10^{18} cm^{-3} n doped In(.3)Ga(.7)As
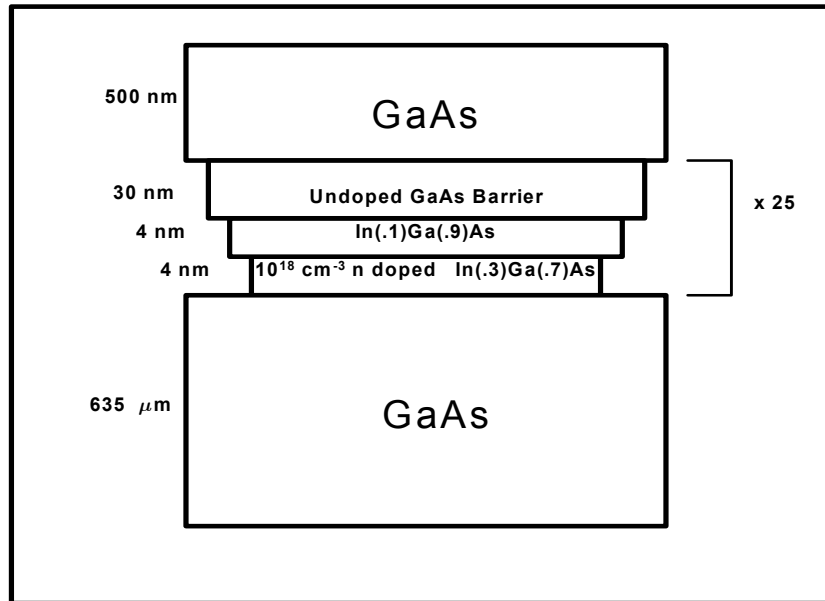
x 25

635 μm — GaAs

Figure 8. Drawing illustrating quantum well structure. The width of each layer schematically represents the bandgap.

THIS PAGE INTENTIONALLY LEFT BLANK

IV. ABSORPTION MEASUREMENT

A.   INTRODUCTION TO FTIR

Prior to fabricating a QWIP, the sample must be analyzed to verify that it meets the design parameters. One of the important parameters is the infrared absorption spectrum of the sample. This is analyzed through the use of Fourier Transform Infrared Spectroscopy (FTIR).

In order to find the wavelengths that the QWIP will absorb and ultimately detect, an infrared spectrum must be created. Traditionally spectrometers use gratings to reflect a small range of wavelengths from a light source onto a detector (this will be referred to as the source spectrum). This allows the user to determine the intensity of light transmitted as a function of wavelength or frequency.

The spectra for this thesis, however, were generated using a Fourier transform infrared spectrometer. FTIR uses optical interference principles to rapidly produce high-resolution spectra. There are two main advantages of FTIR: the multiplex or Fellgett advantage and the throughput or Jacquinot advantage (Bell, 1972).

Because the gratings used in traditional spectrometers pass only a tiny part of the source spectrum, it must scan through the entire range of the grating to acquire a complete spectrum. FTIR uses multiplexing and captures the entire source spectrum during each instant of the scan, greatly reducing the scan time required for a complete spectrum.

Traditional spectrometers restrict the light incident on the detector by means of an aperture and collimating mirrors. This restriction greatly reduces the maximum theoretical resolution of such instruments. The throughput, or *étendue,* advantage of FTIR is that no apertures or mirrors that are present greatly reduce the solid angles incident on the detector so they do not impose such resolution limits.

B. THEORY

Following Bell (1972), the amplitude of light incident on a beamsplitter (as in a Michelson interferometer) is given by

$$E(z,\sigma) = E_0(\sigma)e^{i(\omega t - 2\pi\sigma z)} \qquad (4.1)$$

where E is the electric field at point z, σ is the wave number, ω is the frequency, and t is the time. The two recombining beams have traveled distances of z_1 and z_2 and the amplitude of the recombined beams is (within a multiplicative constant for reflection and transmission of the beamsplitter)

$$E_R = E_0(\sigma)[e^{i(\omega t - 2\pi\sigma z_1)} + e^{i(\omega t - 2\pi\sigma z_2)}]. \qquad (4.2)$$

This gives an intensity of

$$\begin{aligned} I(z_1, z_2, \sigma) &= E_R(z_1, z_2, \sigma)E_R^{*}(z_1, z_2, \sigma) \\ &= E_0^{2}(\sigma)\{1 + \cos[2\pi(z_1 - z_2)\sigma]\}. \end{aligned} \qquad (4.3)$$

Since FTIR uses a broadband source the total intensity for a difference in path length δ can be obtained as

$$I_R(\delta) = \int_0^\infty I(\delta, \sigma) d\sigma$$

$$= \int_0^\infty E_0^2(\sigma) d\sigma + \int_0^\infty E_0^2(\sigma) \cos(2\pi\delta\sigma) d\sigma. \tag{4.4}$$

where $\delta = z_1 - z_2$. Only the sinusoidal component from (4.4) is needed so the intensity can be defined as

$$I_R(0) = 2\int_0^\infty E_0^2(\sigma) d\sigma. \tag{4.5}$$

The interferogram, $b(\delta)$, is then defined as the received intensity as a function of path length difference, and is given by

$$\int_0^\infty E_0^2(\sigma)\cos(2\pi\delta\sigma)d\sigma = I_R(\delta) - 2\int_0^\infty E_0^2(\sigma)d\sigma = I_R(\delta) - \frac{1}{2}I_R(0). \tag{4.6}$$

Finally, to calculate the spectrum, B, one must take the Fourier cosine transform to obtain

$$B(\sigma) = \Im[b(\delta)] \propto E_0^2(\sigma) = \int_0^\infty [I_R(\delta) - I_R(0)]\cos(2\pi\sigma\delta)d\delta. \tag{4.7}$$

C.   EQUIPMENT

As mentioned previously, a Fourier transform spectrometer is a Michelson interferometer combined with the necessary computer to control the source and mirrors, record the data and compute the Fourier transform.   For this thesis, where the required source for the spectrum must be infrared, a Nexus 870 FTIR spectrometer made by Thermo-Nicolet was used.

A Michelson interferometer consists of a broadband infrared light source, a beamsplitter, a moveable mirror,

and a detector as shown in Figure 9 (Hecht, 2002). The moveable mirror changes the beam path length and the detector observes the interference of the beam with itself (in effect producing an analog autocorrelation operation).
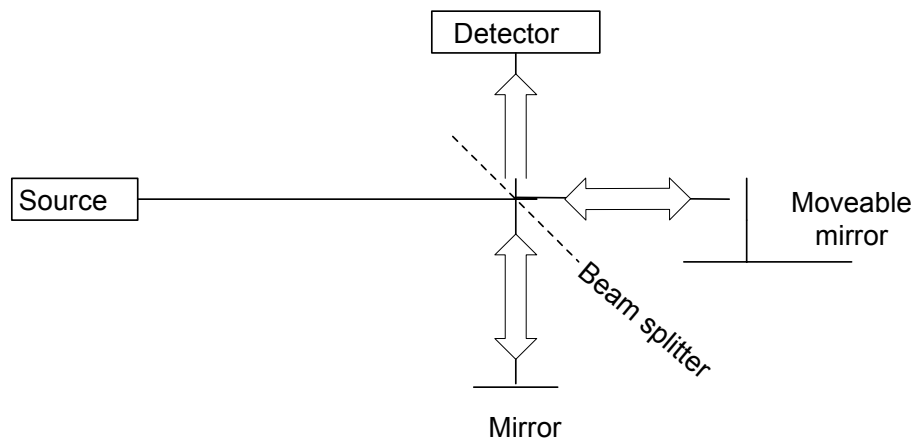
Figure 9. Drawing of a basic Michelson interferometer.

The Nexus spectrometer performs exactly the same task by using a computer to control the moveable mirror and record the detector data. The mirror is moved through its entire range at a speed selected by the user and the detector records the intensity as a function of data point as seen in Figure 10. This process is repeated numerous times and averaged to improve accuracy. The data point axis can easily be converted to a time or distance using the velocity of the mirror and the sampling frequency. The resulting pattern is the interferogram produced by the light that first passes through the sample. Appendix A shows the settings used in OMNIC, the controlling and processing software.

24
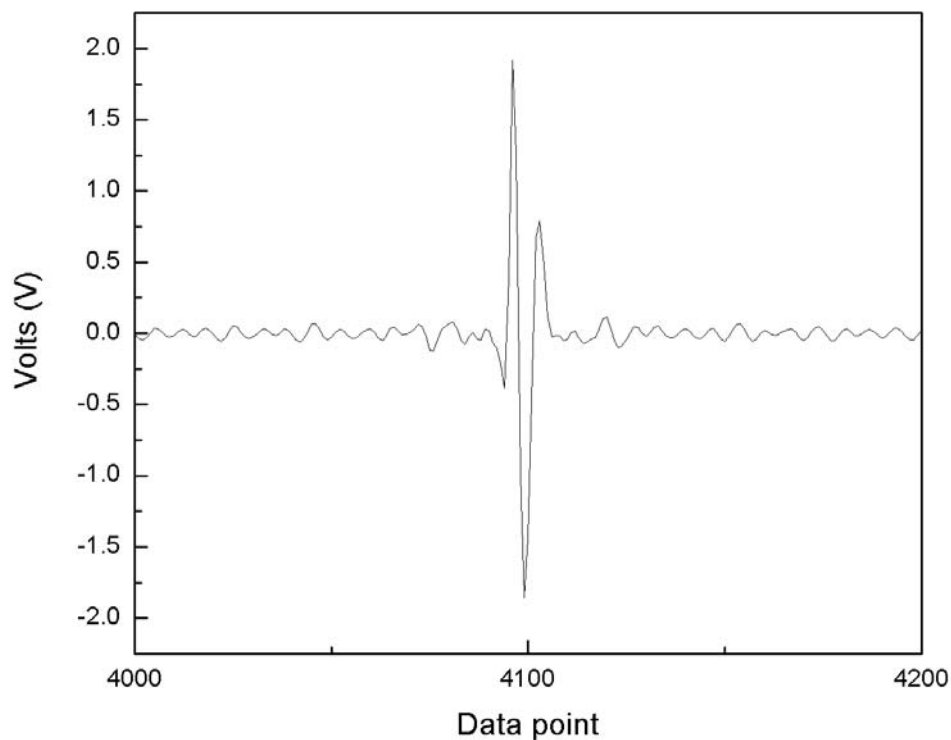
Figure 10.   FTIR Interferogram of sample.

An accurate absorption spectrum must be corrected for atmospheric and other undesired absorption. To do this, a reference (or background) interferogram is acquired immediately prior to each device interferogram. The background interferogram is taken using various methods to eliminate or calculate corrections for various causes of absorption. The difference between the two interferograms is used to obtain the final absorption spectrum that is corrected for absorption by the atmosphere and by the bulk material in the optical path.

25

D.   SAMPLE PREPARATION

As discussed previously, the incident photons must
have a component of polarization in the crystal growth (x)
direction in order to be absorbed by the quantum well.
Since light waves are transverse, light that is normally
incident on a QWIP device will not be absorbed. This can
be overcome by sending light at an angle to the quantum
well structure as illustrated in Figure 11.
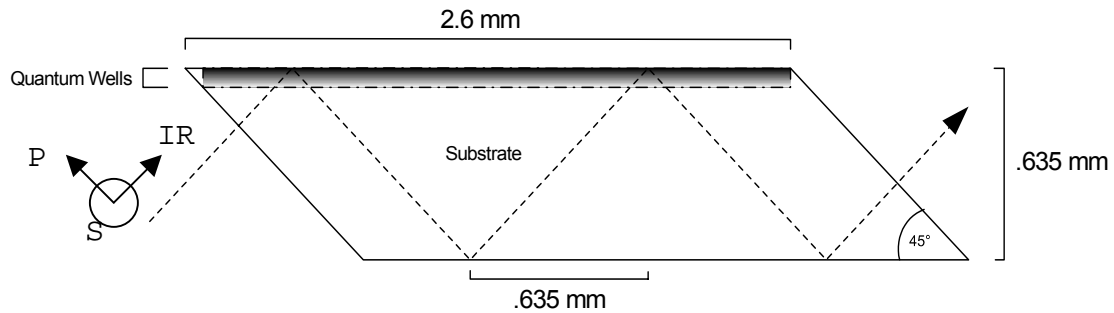
Figure 11.   Waveguide fabricated by grinding the
edges of the sample to 45°.

In the measurement a waveguide is made from the sample
to force light to travel in the required direction. This
is achieved by grinding and polishing the edges of the
sample to make a 45° angle (Figure 11) where the light is
internally reflected several times and is absorbed during
each pass through the multiple quantum wells.

For the device used in this thesis, grinding was
accomplished using a South Bay Technology, Inc. (Model 900)
Grinder/Polisher.   The sample was secured with wax to a
holder that maintains an angle of 45° with the grinding

26

surface and held towards the middle of the disk, which turned at approximately 50 - 80 rpm. Two opposing edges were ground using a 600 grit carbide disk with a grain diameter of 14 microns. The 45° faces were then polished using a 1200 grit (grain diameter of five microns) carbide disk followed by a polishing cloth covered with aluminum powder with a grain diameter of 0.3 microns.

The final waveguide was 2.55 mm high, 13 mm long, and 0.64 mm wide. Once cut and polished, the sample was inserted into a gold plated vice that channels the incident beam of the spectrometer into the waveguide. The light enters the device normal to the 45° face, reflects through the device, and is transmitted out the opposing face into the spectrometers detector.

E. DATA COLLECTION

A wire-grid infrared polarizer was used to obtain the background spectrum (including the absorption in the GaAs substrate) since the quantum wells do not absorb when the light polarization is parallel to the layers. The polarizer used was a 22 mm diameter Harrick Scientific Wire Grid polarizer on a KRS-5 substrate with 95% efficiency at 5 μm. It is effective from 2 μm to 35 μm.

The absorption spectrum was taken using the spectrometer settings listed in Appendix A. The spectrometer was set to automatically scan and calculate a background spectrum prior to taking the device spectrum. The background spectrum was taken with the polarizer set to transmit only S-polarized light, which was not absorbed by

27

the quantum wells. This had the effect of extracting the
absorption of the beam path and the substrate. The sample
spectrum was then taken using P-polarization to maximize
absorption by the quantum wells. It was compared to the
background absorption to compute the overall spectrum of
the quantum well structure.
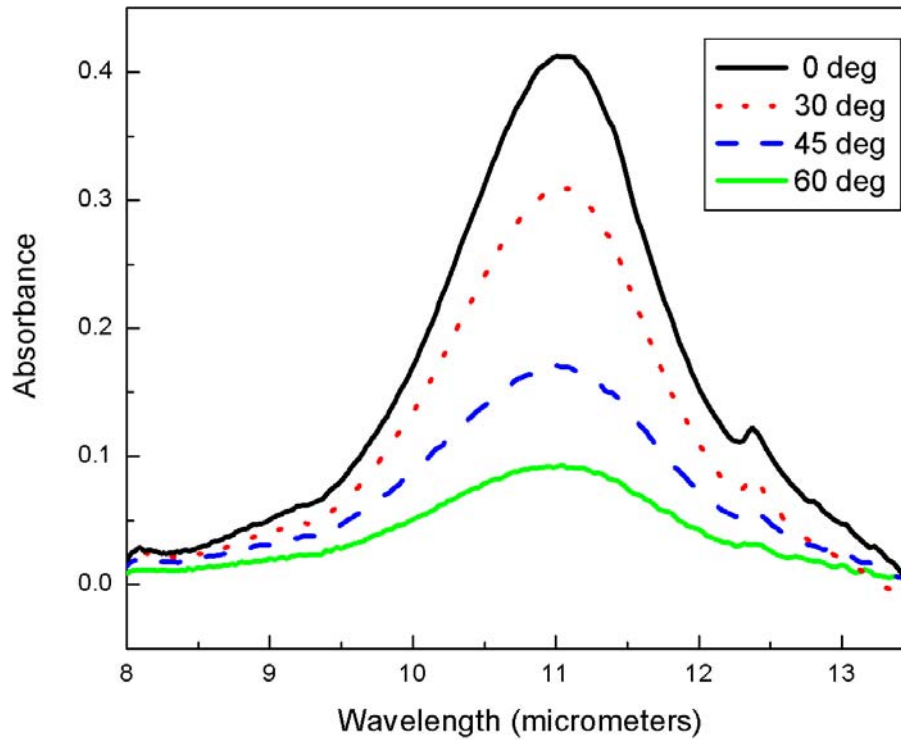

Figure 12. Polarization   dependence   of
absorbance of 25 InGaAs quantum step wells.
Peak absorbance is 0.41 at 900 cm^{-1} (11.1 μm
wavelength).

In order to ensure the absorption was only due to the
quantum wells, the sample absorption was taken using
polarizations of 30, 45, and 60-degrees relative to the P-
polarization. Figure 12 shows that as the polarization

28

angle increases the absorption in the quantum wells decreases as expected.   The peak absorption occurs at a wave number of 900 cm^{-1} with an amplitude of 0.41 and a bandwidth (full width at half maximum or FWHM) of 183 cm^{-1}. This equates to a peak absorption at 11.1 μm and a bandwidth of about 1.6 μm.

Given that the absorbance, A, is

$$A = -\log_{10}[T] \tag{4.8}$$

and

$$T = e^{-\alpha L} , \tag{4.9}$$

the absorption coefficient is found to be given by

$$\alpha = \frac{A}{L \cdot \log_{10} e} . \tag{4.10}$$

The path length (L) through the quantum wells is then found to be

$$L = nNw\cos(45^\circ) \tag{4.11}$$

where n is the number of quantum wells in each pass, N is the number of passes, and w is the period of quantum wells. For this sample, the absorption coefficient was found to be 1800 cm^{-1} which is comparable with that observed in bulk semiconductor.

THIS PAGE INTENTIONALLY LEFT BLANK

V. FABRICATION

A. ETCHING

In order to characterize the electrical and optical properties the wafer must be processed into individual devices. The process is commonly used for semiconductor processing and was conducted by Mei Ting at the Nanyang Technological University (NTU) in Singapore.

In general, the process of etching begins by coating the surface of the wafer with photoresist (Zhou, 2001). Next, a mask is placed over the photoresist and exposed to ultraviolet (UV) light to define the devices. After developing, the wafer is wet etched to expose the buffer layer. Then, the remaining photoresist is removed. The processed wafer contains devices with dimensions ranging from 80x80 to 300x300 μm^2. The 300x300 μm^2 devices were used in this study.

Ohmic (metallic) contacts must then be placed at both sides of the series of quantum wells. This is done by placing metal (usually gold or a gold alloy) on top of the contact layer consisting of n-doped GaAs and located above each device. The other contact is a grid of metal contact material on top of the buffer layer that supports the array of devices. This grid is referred to as the ground plane of the device. The metalization is carried out by defining areas to be metalized using a mask and repeating the steps used in the etching of mesas. Then the metal is evaporated onto the unmasked sections of the wafer that define the ground plane and the device contacts.

B.   DEVICE ASSEMBLY

Once the individual devices were etched and contacts deposited on the cap layer it had to be fitted to a package that could allow light to hit the devices and current to be extracted for further processing.   The first step in the process was to cut a 45° facet similar to that used in the FTIR measurement.

The facet was cut such that the largest devices (.3 mm x .3 mm square mesas) were located directly in the path of incident radiation.   As shown in Figure 13, there are several devices of the largest size located on the edge directly over the waveguide.
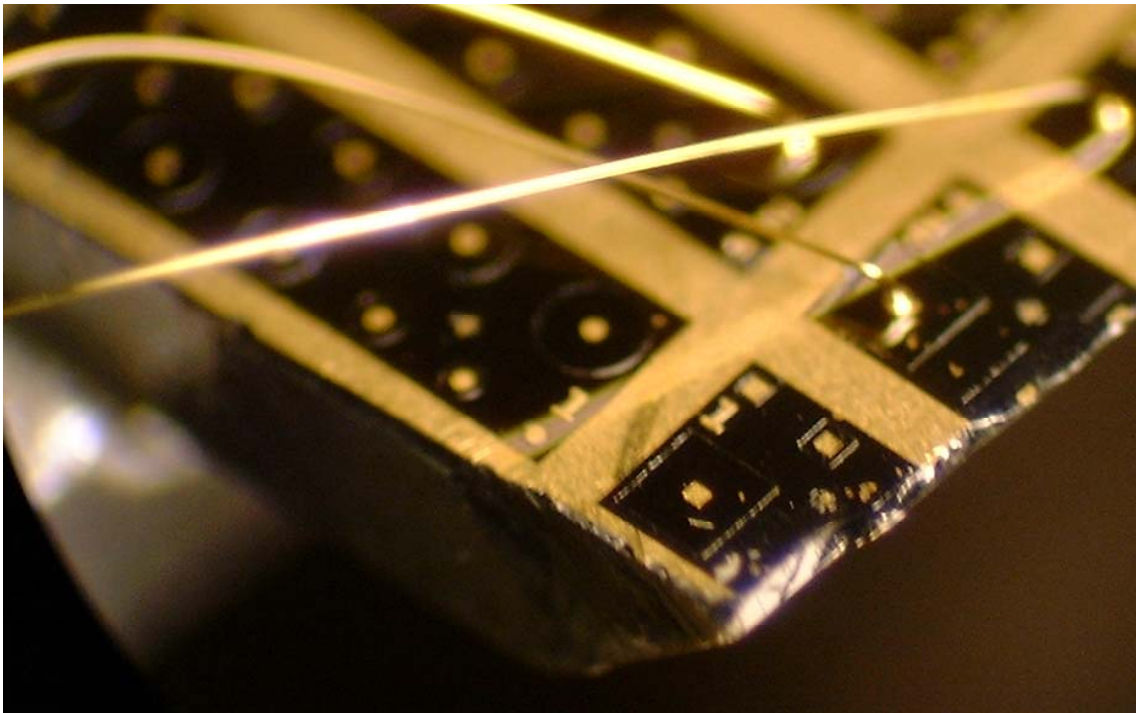

Figure 13.   Microscopic photograph of topside of sample.   The gold dots are ohmic contacts surrounded by the larger mesas (devices).

After creating the 45° facet, it was mounted on a chip holding package and wired to the package leads. An Addison Engineering, 28 lead, side braze, ceramic package with a 0.310 inch square cavity was used. It was cut in half so the 45-degree facet could go hang over the edge and be exposed to the incident light.

The device was secured to the package with Cicuit Works brand two-compound conductive epoxy. Once mounted, the package was placed on the heated wire bonder stage set to 150 °C for 10 minutes then allowed to cool at room temperature overnight for curing the epoxy.

C. WIRE BONDING

Finally, the metal contacts were connected to the bonding pads of the chip package using a Kulicke & Soffa Industries (Model 4524A) wire bonder. This machine allows the user to maneuver the chip package under a ceramic tip through which gold wire passes. The end of the wire is sparked to create a gold ball that is bonded to a metal contact in a process called ball bonding.

In ball bonding, the gold ball is placed directly over the device's metal contacts then pressed down and lightly vibrated to ensure a good bond. The device is then moved so the contact pad on the chip carrier is directly below the ceramic wire bonding tip and the wire is again pressed onto the device and bonded, breaking the wire at the end. Once the tip is elevated above the device, it is again sparked to create a ball to use for the next bond.
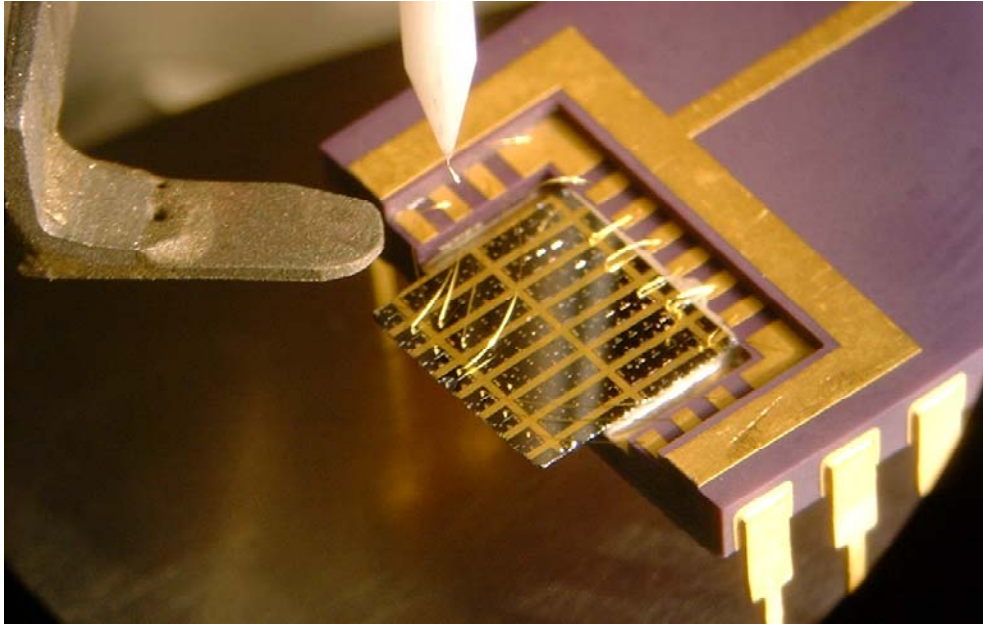
Figure 14.   Photograph of device mounted on chip
package. Wires from devices to package can be
seen as well as white ceramic bonding tip.

The wire bonder settings were optimized using a spare
device so that individual devices were not damaged due to
excessive force, power, or heat.   It appeared most
effective to lower the tip to the first search height, then
slowly change the wire bonder's search height setting until
the ball almost touched the device to ensure accurate
placement.   Care was then taken to reset the search height
so the tip or a device was not damaged during subsequent
bonds.   Appendix B contains the optimized wire bonder
settings for this device assuming the ball is placed on the
device and not on the package.

It was critical to plan the placement of the wires
prior to beginning the bonding process.   Because the
useable devices were at the far end of the sample from the
package, the wires were quite long and could easily be

crossed. Wires must also be connected to the ground plane (a grid on the device used for this thesis). The most effective method seemed to be to align the wire bonder stage for each bond so that it could be moved straight backward or forward.

For this thesis, six devices in the row closest to the edge and two in the second row were bonded to the eight bonding pads closest to the end. The remaining bonding pads were bonded to the ground plane at various points.

Measuring the room temperature resistance between a device and ground can initially check the wire bonds and devices. The room temperature resistance of the device ultimately used is 11.4 Ω.

THIS PAGE INTENTIONALLY LEFT BLANK

VI. DEVICE PERFORMANCE

In order to understand the performance of a detector there are several characteristics that must be analyzed. These include both the electrical and optical measurements.

A.   I-V MEASUREMENT

The first parameter used to characterize a detector is the analysis of current drawn for various bias voltages (called I-V curves). I-V curves can illustrate where the device is most sensitive to changes in voltage in order to determine an appropriate operating range. They are also used to determine the amount of leakage current at various temperatures, which provides information on the barrier height from the ground state of the quantum well.

1. Equipment

I-V curves were generated using an Agilent Technologies 4155B Semiconductor Parameter Analyzer with a 16442A Test Fixture. Equipment setup and use of the Semiconductor Analyzer as well as the cooling chamber required to minimize thermal excitation is described in detail in Hickey (2002).

The package was mounted on the cold-head of the cooling chamber using a brass adapter that held the waveguide normal to the incident illumination as seen in Figure 15. The connecting wires were fastened to package leads corresponding to the devices closest to the center.
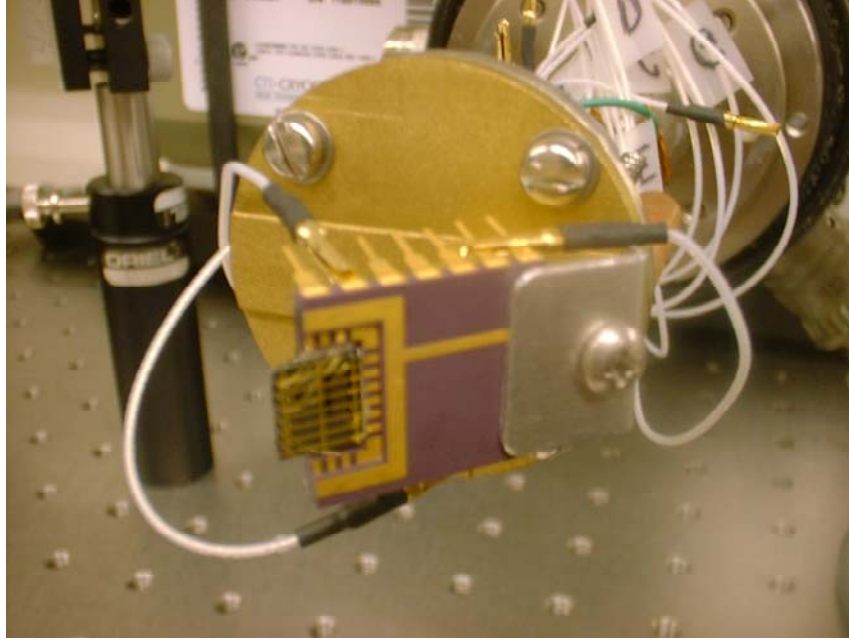
37

Figure 15. Device mounted on cold head of refrigerator with signal processing wires attached. Light from a monochromator was incident from the left.

Once connected and checked for inadvertent grounding or shorting, the cooling chamber was evacuated to approximately 1 mbar and then cooled to 10 K.

2. Data Collection

As discussed previously, QWIPs must be cooled to minimize thermionic emission and, therefore, dark current. In order to obtain the dark current it is necessary to block the background infrared radiation that enters the field of view of the detector. By surrounding the device with aluminum foil inside the cooling chamber, incident radiation from outside is blocked and the aluminum foil

only emits radiation at levels proportional to the temperature of the aluminum foil (~10 K), which is negligibly small.

I-V curves were first taken with aluminum foil covering the device and cold head of the chamber at temperatures ranging from 10 K through 110 K in 10 K steps. Using the pre-installed Diode setup of the Parameter Analyzer with voltages between ±1 V and current limited to 1 mA, I-V curves were generated as seen in Figure 16. Forward bias refers to positive potential placed on the cap layer contact.
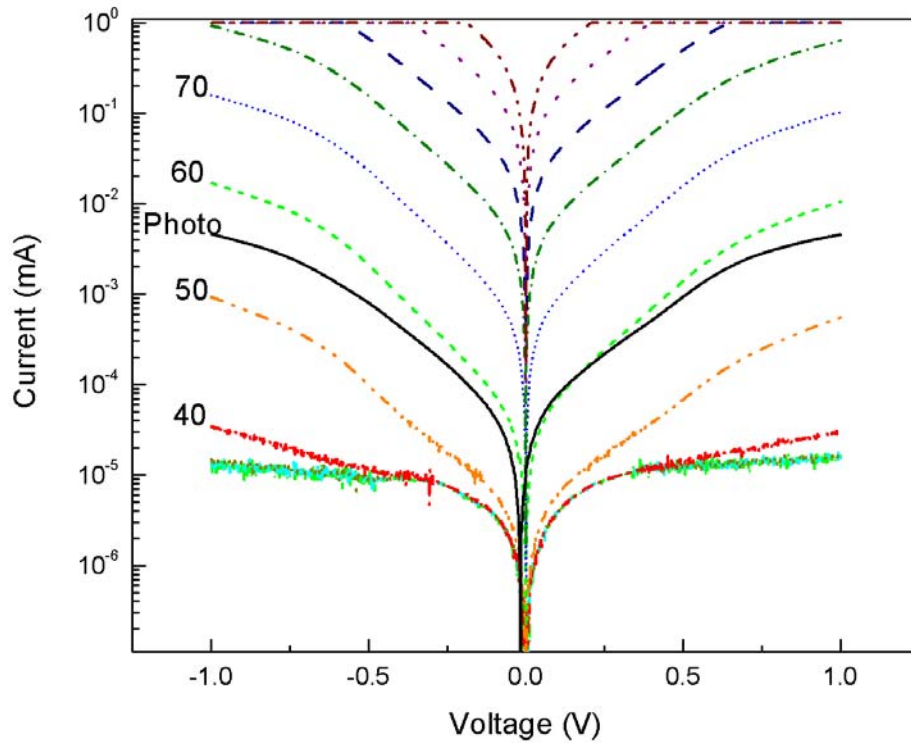

Figure 16.   Plot of dark current versus voltage for various temperatures in QWIP.

After the dark current measurements for various temperatures, the aluminum foil was removed. A single I-V curve was then generated at 10K while background radiation was allowed to illuminate the device (also shown in Figure 16). There are two important features to note when this photocurrent measurement is plotted against the dark current measurements: it lies between 50 and 60 K dark current, and there is a shift of the zero-current voltage of approximately -18 mV.

Since a room temperature background causes a photocurrent greater than the dark current at 50 K, cooling the device lower than 50 K will not lower the noise generated by the detector and would be a wasted effort in an operational setting. The background-limited performance of the device used in this thesis occurs at approximately 55 K where the dark current is nearly the same as the background generated photocurrent.

The shift in zero-current voltage is likely due to the asymmetry of the quantum well and its creation of an internal electric field as shown by the wave functions predicted through Lantz' (2002) program (Figure 17). This requires further investigation, but is likely due to the current induced from the large background infrared photons.
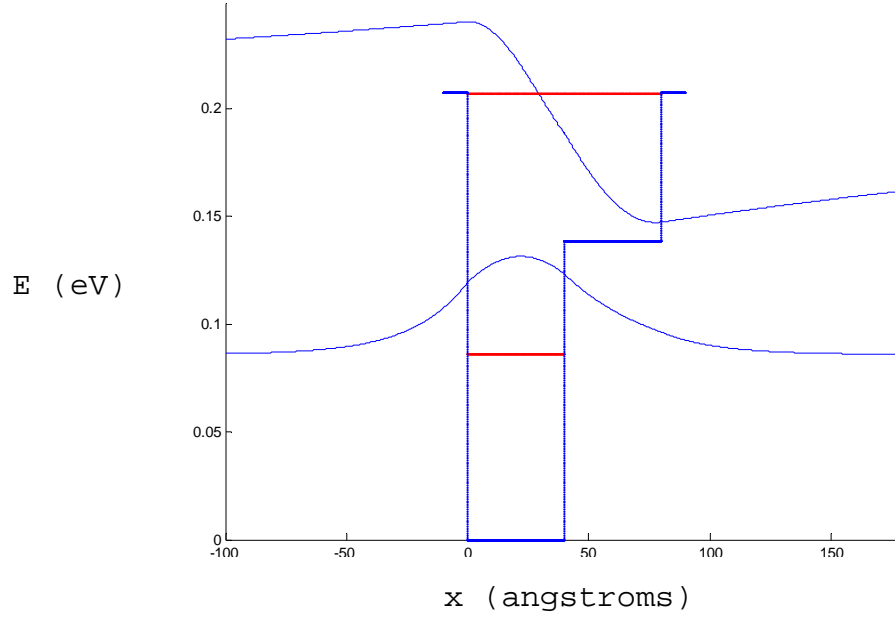
Figure 17. Step potential well with wave functions superimposed.

3. Barrier Height Calculation

As explained in Hickey (2002), the barrier height can be calculated using the data taken to generate the I-V curves. The barrier height determines the minimum photon energy required to excite an electron into the continuum and contribute to the photocurrent. Given that

$$E = \frac{hc}{\lambda} \qquad (6.1)$$

the minimum energy defines the maximum, or cutoff, wavelength of the detector. It can be shown that the leakage current at a constant bias is given by (Levine, 1993, p. R20)

$$I(T) \propto Te^{-\frac{(V_B - E_F)}{kT}} \qquad (6.2)$$

41

where V_B is the barrier height measured from the ground state of the quantum well and E_F is the Fermi energy.

Holding bias constant and plotting the value of

$$\ln[\frac{I(T)}{T}] \quad vs. \quad \frac{1}{T} \qquad (6.3)$$

for several different temperatures should yield a straight line as shown in Figure 18. The slope of this line is given as
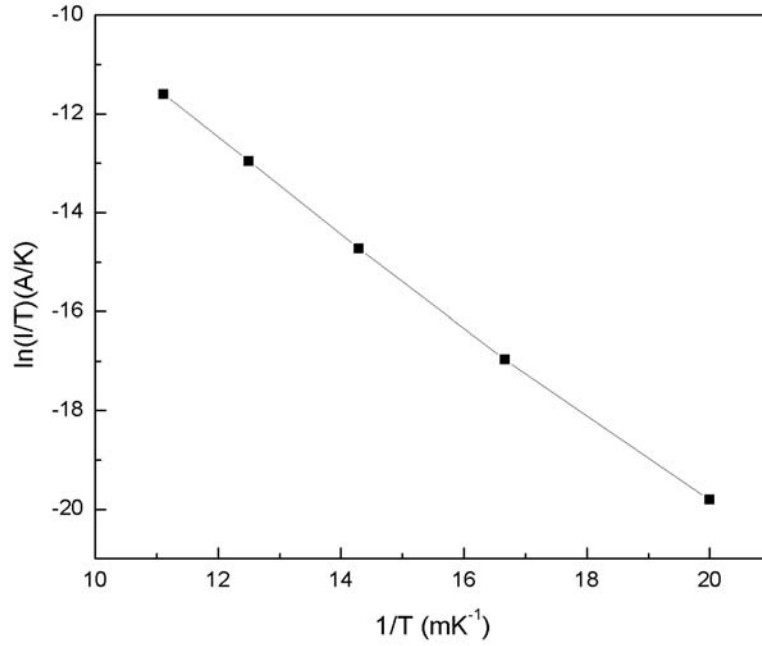
$$\frac{V_B - E_F}{k_B} . \qquad (6.4)$$

Figure 18. Plot of ln(I/T) vs. 1/T at 0.6 V bias. The slope of this line is $\dfrac{V_B - E_F}{k_B}$.

As shown in Table 2, an average value of $V_B - E_F$ (when plotted for biases between 0.2 and 0.6 V in steps of 0.05 V) was found to be about 80 meV.

Bias (V)	$V_B - E_F$ (eV)
0.6	0.080
0.55	0.080
0.5	0.081
0.45	0.081
0.4	0.081
0.35	0.074
0.3	0.073
0.25	0.081
0.2	0.080

Table 2 Table of $V_B - E_F$ for biases between 0.2 V and 0.6 V.

The Fermi energy in the doped quantum well can be obtained using (Karunasiri, 1996)

$$E_F = \frac{n_D \pi \hbar^2 L_w}{m_w^*}$$

(6.5)

where n_D is the doping level in the quantum well, L_w is the spatial width of the bottom of the well, and m_w^* is the effective mass of electrons in the well calculated by Vegard's Law (43×10^{-33} kg). This yielded a Fermi energy of 20 meV resulting in a barrier height of 99 meV. This amounts to a long-wave cutoff of about 12.5 μm.

43

B.   PHOTOCURRENT

In order to use a real infrared detector the user must be able to equate the voltage or current produced by the device to an actual intensity. The value used to compare different detectors is called the responsivity and can be presented as the voltage or current per unit incident power. Responsivity was calculated in terms of current because the photovoltaic response of the device is minimal due to the exceedingly short lifetime of electrons in the excited state. Another critical parameter of an IR detection device is the normalized detectivity, or D*, which has the information about the ultimate sensitivity of the detector.

1. Equipment

The equipment used for responsivity measurement was originally set up and calibrated as part of an earlier thesis (Herdlick, 2002). The specific set up and usage of the equipment and software can be found there, with a few exceptions that are explained below.

The major components included a light source that approximated a blackbody centered either in the visible or infrared region, a monochromator consisting of six filters and three gratings to scan the wavelengths in the various bands, two lock-in amplifiers that are frequency referenced to an optical chopper, a beam splitter (grating-type), an electronics breadboard for circuit manipulation, and a power supply for biasing the device.

Instead of reading the device while scanning through the desired wavelength band, the LABVIEW software created

in Herdlick (2002) was altered to scan to a discrete wavelength, pause, read each lock-in amplifier in series, and then scan to the next wavelength. This alleviated timing variations caused by the computer control and communications interruptions. Grating and filter changes were switched into an automatic mode and the scan feature was realigned to occur in series – each step waiting for the previous one to be reported as complete.

As described in the previous thesis (Herdlick, 2002), the beam was split so the device response can be compared to a flat-response reference to account for variations in power emitted by the source or absorbed along the optical path. The reference used has a constant responsivity of 1000 V/W using an area of 5 mm x 5 mm. This provides a real time determination of power incident on the detector.

2. Responsivity and Detectivity (D*) Calculation

The responsivity, $\Re$, is defined by (Dereniak and Boreman, 1996):

$$\Re = \frac{V}{\phi} ,$$

(6.6)

where ϕ is the flux or power incident on the device, and V is the measured voltage generated by the photocurrent. The flux incident on the reference detector can be defined as

$$\phi_R = \frac{V_R}{\Re_R}$$

(6.7)

where V_R and $\Re_R$ are the photovoltage produced by the reference detector and its responsivity, respectively. The intensity on both the reference detector and test device is

45

nearly the same by virtue of the beamsplitter selection. Therefore, the flux incident on the test detector, ϕ_D, is proportional to the fractional illuminated area of the device and of the reference, or

$$\phi_D = \phi_R \frac{A_D}{A_R} = \frac{V_R}{\mathfrak{R}_R} \frac{A_D}{A_R} \qquad (6.8)$$

where A_D and A_R are the area of the test and reference detectors, respectively.

Since ϕ_D is the intensity incident on the outer window of the test detector chamber, the light incident on the device had to be corrected to take into account the reflections at the window and the 45° facet. The transmission coefficient of zinc selenide, T_{ZnSe}, was deduced from a graph and linearized between 800-1000 nm for the NIR region, and 8-10, 10-11, and 11-12 μm for the IR region yielding values between 0.6 and 0.73. The transmission coefficient at the air/GaAs interface was calculated using (Kasap, 2002)

$$T_{GaAs} = 1 - \frac{(n_1 - n_2)^2}{(n_1 + n_2)^2} = .68 \qquad (6.9)$$

where n_1 and n_2 are the index of refraction of GaAs (3.6) and air, respectively.

Since the responsivity was to be given as current as a function of incident power, V in Eq. 6.5 was replaced by I, the photocurrent produced. By using the circuit shown in Figure 19, one could measure the voltage across the load resistor R and calculate the current through it by Ohm's Law. Since R was in series with the test device, the

current through each was the same. This had to be done because the detector is a photoconductor and its resistance depends on the incident power.
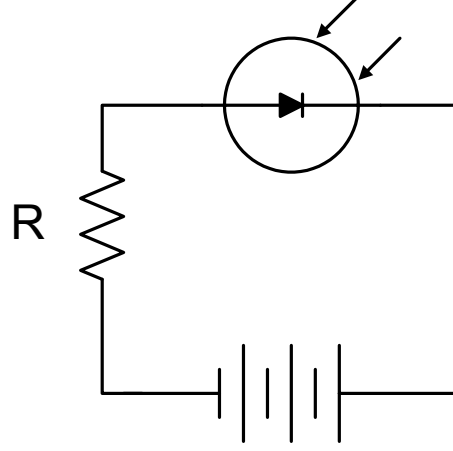

Figure 19. Diagram of circuit used to measure photocurrent.

Lastly, the power incident on the test device is reduced by a factor of $1/\sqrt{2}$ due to the 45° angle between the detector area and the incident beam. This yields a final equation for the responsivity of the device given by

$$\Re_D = \frac{V_\Omega}{R} \frac{\Re_R}{V_R} \frac{A_R}{A_D} \frac{2}{T_{GaAs}T_{ZnSe}\sqrt{2}}$$

(6.10)

where V_Ω is the voltage across the load resistor.

Detectivity is a statement of the signal-to-noise ratio (SNR). It relies on another factor called the noise-equivalent-power (NEP). The NEP of a device is given as (Dereniak and Boreman, 1996, p.203)

$$NEP = \frac{I_n}{\Re_D}$$

(6.11)

47

where I_n is the noise current whose major contributions are noise from thermal motion (Johnson noise), generation and recombination of electrons (G-R noise), and noise from electrons traversing a potential barrier (shot noise). D* is then defined as

$$D^* = \frac{\sqrt{A_d \cdot \Delta f}}{NEP}$$
$$= \frac{\Re_D \sqrt{A_d \cdot \Delta f}}{I_n}.$$

(6.12)

Since the detector that we fabricated is a photoconductor the main contribution to the noise comes from the generation and recombination of carriers. The corresponding noise current is given by

$$I_n = \sqrt{4eGI_D \Delta f}$$

(6.13)

where G is the optical gain and considered to be unity in this case, I_D is the total current through the device (photocurrent + dark current) and Δf is the frequency bandwidth which is usually taken to be 0.1 (Levine, 1993, p. R26). This yields a final detectivity equation of

$$D^* = \Re_D \sqrt{\frac{A_D}{4eGI_D}} \left(\frac{cm\sqrt{Hz}}{W} \right).$$

(6.14)

3. Photoresponse Data

As shown in Figure 20 and Figure 21, the maximum responsivity of the device was 0.036 A/W in the designed NIR band and 0.69 A/W in the IR band. The peak responsivity for forward bias occurred at 832 nm with a bandwidth of approximately 125 nm in the NIR and remained detectable through approximately 960 nm. For the IR band, the peak responsivity occurred at 10.93 μm with a bandwidth of approximately 1.3 μm in the IR.
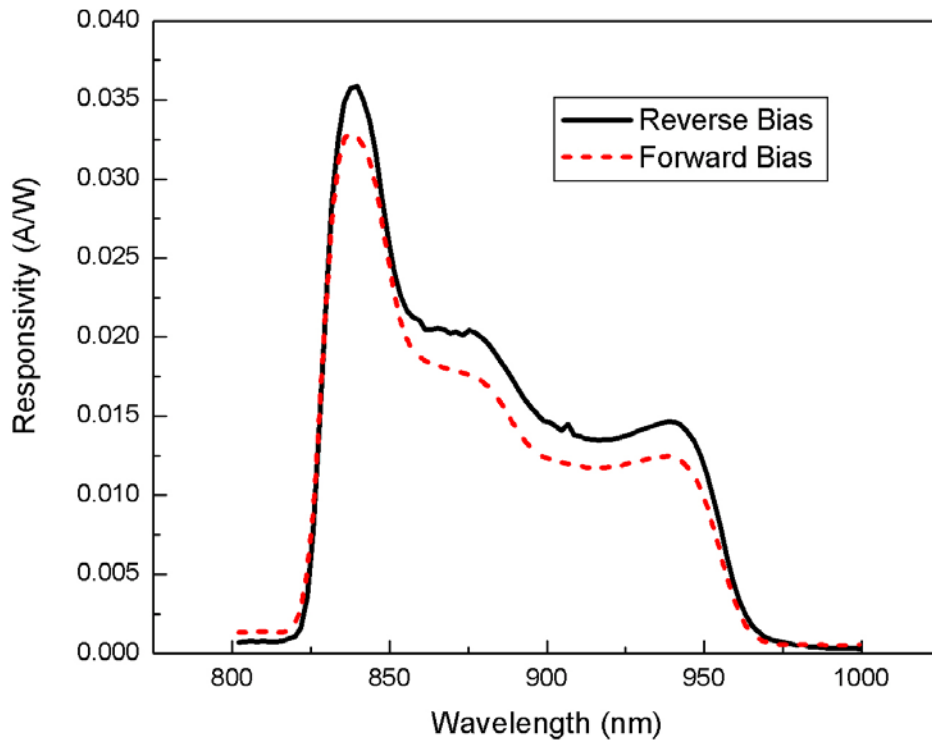

Figure 20. Responsivity versus wavelength of forward and reverse biased QWIP in the NIR band.
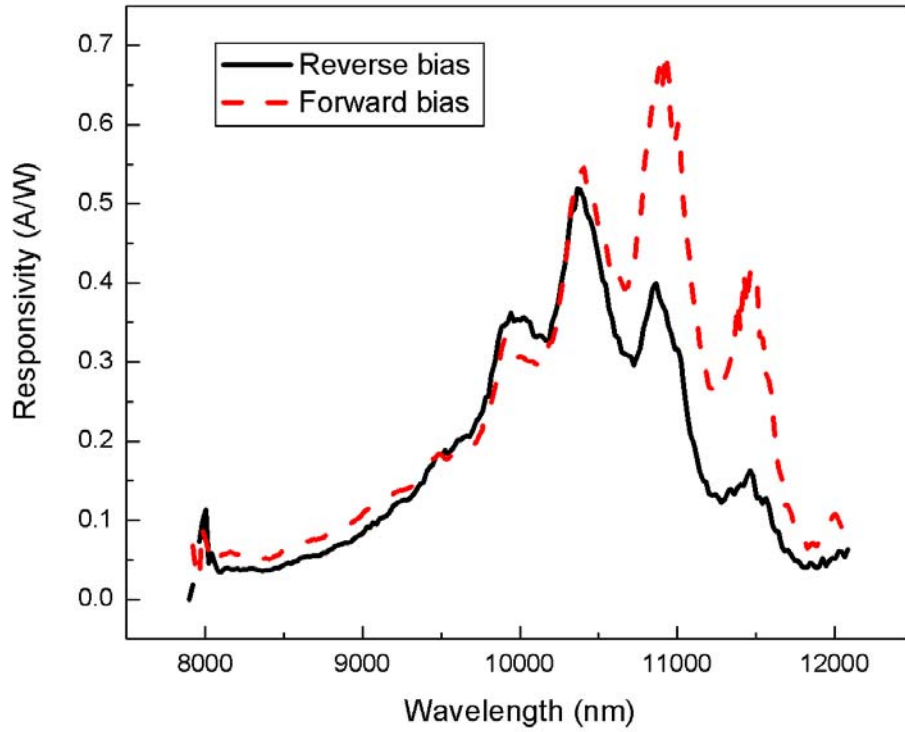
Figure 21. Responsivity versus wavelength of forward and reverse biased QWIP in the mid-IR band.

The responsivity was slightly reduced for a 1 V reverse bias and further reduced for smaller reverse biases as expected due to the reduction of drift velocity of the excited carriers. The linear Stark effect associated with step quantum wells is responsible for the significant peak shift towards longer wavelengths under forward bias (Mii, *et al.*, 1990). Bias dependence is shown in Figure 22 and **Error! Reference source not found.**. The long-wave cutoff above 12 μm agrees with the calculated barrier height of 99 meV.
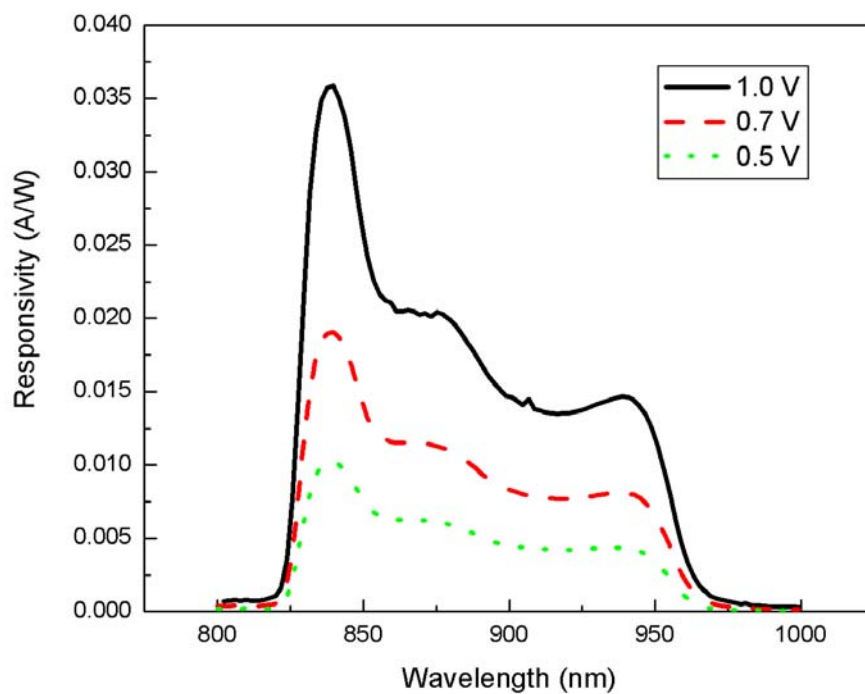
Figure 22. Bias dependence of responsivity in the NIR band.
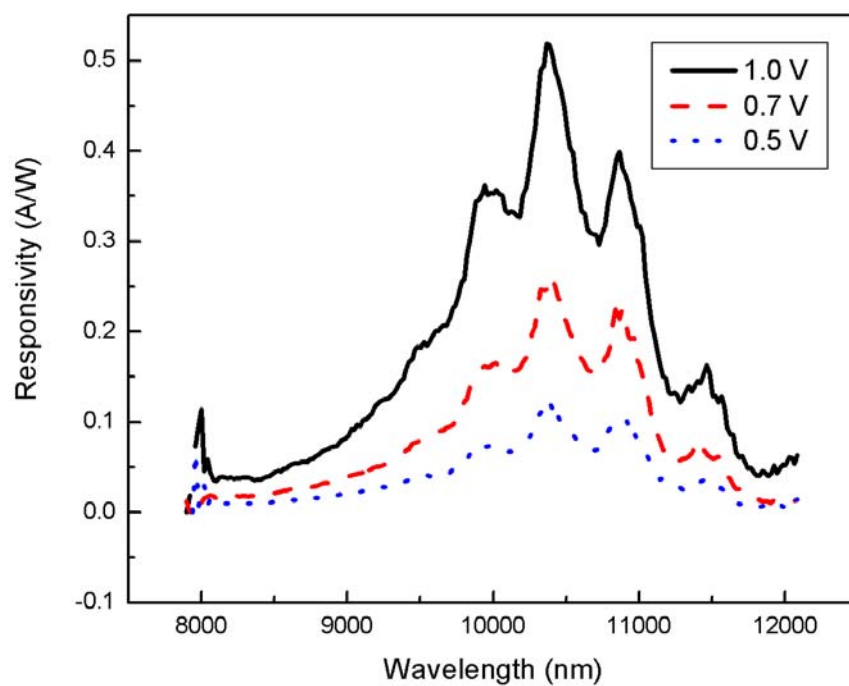
Figure 23. Bias dependence of responsivity in the IR band.

The maximum detectivity, D*, was then calculated to be 3.4×10^{10} cm$\sqrt{\text{Hz}}/W$ in the NIR band and 6.5×10^{11} cm$\sqrt{\text{Hz}}/W$ in the IR band at 10 K assuming no background infrared radiation. D* at the background limited point (D^*_{BLIP}) was 2.0×10^9 cm$\sqrt{\text{Hz}}/W$ in the NIR and 3.9×10^{10} cm$\sqrt{\text{Hz}}/W$ in the IR at 55 K. The decrease in D* at 55 K is due to the larger leakage current.

VII. CONCLUSION

In this thesis, a device was designed to ultimately detect a laser designator operating at 1.06 μm and infrared radiation near 10 μm. The final design was comprised of 25 quantum step wells that were used to break the symmetry of typical square well devices in order to allow a normally forbidden transition from the first valence band energy state to the second conduction band energy state. This interband transition combined with an intersubband transition allowed for the detection of light in the near and mid-infrared wavelength bands.

The quantum well sample was fabricated and successfully demonstrated to absorb light in the IR band with a peak at 11.1 μm and a bandwidth of 1.6 μm. The absorption coefficient was 1800 cm^{-1}. It was then wet etched into a 300 μm x 300 μm mesa structure, fitted with ohmic contacts, and wire bonded to a ceramic carrier.

Current versus voltage analysis found a dark current of 1.6 x 10^{-8} A at 1 V bias at 10 K and a background photocurrent of 4.6 x 10^{-6} A at 10 K. The background-limited performance of the device occurs at approximately 55 K. The measured barrier height of the well using temperature dependent I-V data is about 99 meV.

Responsivity was then measured for both bands. A maximum responsivity was measured to be 0.036 A/W in the designed NIR band and 0.69 A/W in the IR band. The peak responsivity for forward bias occurred at 832 nm with a bandwidth of approximately 125 nm in the NIR and remains

detectable through approximately 960 nm. For the IR band, the peak responsivity occurs at 10.93 μm with a bandwidth of approximately 1.3 μm in the IR. The estimated barrier height using I-V data is in good agreement with the observed long wavelength cut-off of the detector at 12 μm.

Detectivity was then calculated to be 3.4 x 10^{10} cm$\sqrt{\text{Hz}}/W$ in the NIR band and 6.5 x 10^{11} cm$\sqrt{\text{Hz}}/W$ in the IR band. D* at the background limited point (D*$_{\text{BLIP}}$) was 2.0 x 10^{9} cm$\sqrt{\text{Hz}}/W$ in the NIR and 3.9 x 10^{10} cm$\sqrt{\text{Hz}}/W$ in the IR.

Where possible, the measured parameters were compared with earlier work presented in Hickey (2002) and Levine (1993). The absorption coefficients in other works were seldom greater than 1000 cm^{-1} compared to 1800 cm^{-1} found in this thesis.   This is due to the 50% higher doping levels we used in the step quantum wells. The maximum D* values were approximately a factor of 10 smaller than most presented in Levine (1993, p. R31) but D*$_{\text{BLIP}}$ values were comparable. The devices presented in such texts utilized only symmetrical quantum wells using smaller biases.

Clearly the device is able to perform as both a near and mid-infrared detector using the planned design. Further research is required to optimize the material structure (likely using more In in the lowest well to include 1.06 μm in the detectable band). The experimental set-up can be further improved by using a different type of beam splitter to remove the observed interference effects.

APPENDIX A

OMNIC FTIR SETTINGS

TAB	SETTING	VALUE	UNITS
Collect	Scans	32	
	Resolution	4	wavenumbers
	Format	Absorbance	
	Data spacing	1.928	cm-1
	Correction	None	
	Atmospheric suppression	None	
	Preview	No	
Bench	Gain	8	
	Velocity	1.581	cm/s
	Aperture	100	%
	View	Min/Max	
	Single Beam	No	
	Tone	No	
	Compartment	Main	
	Detector	DTGS TEC	
	Beamsplitter	KBr	
	Source	IR	
	Accessory	Transmission E.S.P.	
	Window	No	
	Shuttle	No	
	Range	4000-400	cm-1
Quality	Spectrum View		
	Peaks	50	%
	Totally Absorbed Peaks	50	%
	Fringe	80	%
	Derivative Peaks	N/A	
	Base error	50	%
	CO_2	10	%
	H_2O	10	%
Advanced	Zero-fill	None	
	Apodization	Happ-Genzel	
	Phase Correction	Mertz	
	Filters	Auto	
	Spacing	Auto	

THIS PAGE INTENTIONALLY LEFT BLANK

APPENDIX B

Optimized Settings for K&S 4524AD Wire Bonder

Device bond

Power	1.25
Time	5.0
Force	0.6

Chip carrier bond

Power	1.4
Time	5.0
Force	2.6

Other

Loop	5.1
Tail	8.0
Ball	3.7
Mode	Standard
Time	Short
Temp	115

THIS PAGE INTENTIONALLY LEFT BLANK

LIST OF REFERENCES

Bell, R. J., *Introductory Fourier Transform Spectroscopy*. pp. 2. Academic Press, Inc., 1972.

Dereniak, E.L. and Boreman, G.D., *Infrared Detectors and Systems*. p. 70. John Wiley & Sons, Inc. 1996.

Griffiths, David J., *Introduction to Quantum Mechanics*. Chapter 2. Prentice Hall, Inc. 1995.

Herdlick, Brian E., *Computer-Controlled Photodetector Characterization System (Design and Construction),* Master's Thesis, Naval Postgraduate School, Monterey, California, December 2002.

Hecht, Eugene, *Optics*. 4th Ed. p. 408. Pearson Education, Inc. 2002

Hickey, Thomas R., *Temperature Dependence of Dark Current in Quantum Well Infrared Detectors,* Master's Thesis, Naval Postgraduate School, Monterey, California, June 2002.

Karunasiri, G., "Thermionic emission and tunneling in InGaAs/GaAs quantum well infrared detectors," *J. Appl. Phys*., **79**, pp.8121 – 8123, 1996.

Kasap, S. O., *Principles of Electronic Materials and Devices*. McGraw-Hill Companies, Inc. 2002

Kasap, S. and Ruda, H., *Illustrated Dictionary of Electronic Materials and Devices*, Concise Student Edition, v.2, S.O. Kasap, 2002.

Lantz, Kevin R., *Two-Color Photodetector Using An Asymmetric Quantum Well Structure,* Master's Thesis, Naval Postgraduate School, Monterey, California, June 2002.

Levine, B. F., "Quantum-well infrared photodetectors." *J. Appl. Phys., **74**, 1993.

Mii, Y. J., Karunasiri, R. P. G., Wang, K. L., Chen, M., and Yuh, P. F., "Large Stark shifts of the local to global state intersubband transitions in step quantum wells." *Appl. Phys. Lett., **56**, pp. 1986 – 1988. 1990.

Mii, Y. J., Wang, K. L., Karunasiri, R. P. G., and Yuh, P. F., "Observation of large oscillator strengths for both 1-2 and 1-3 intersubband transitions of step quantum wells." *J. Appl. Phys.*, **56**, pp. 1046 – 1048, 1990.

Schneider, H, Schönbein, C., and Bihlmann, G., "Voltage-tunable two-color detection by interband and intersubband transitions in a p-i-n-i-n structure." *Appl. Phys. Lett.*, **68**, p. 1832, 1996.

Singh, J. *Physics of Semiconductors and their Heterostructures*, pp. 184-185, McGraw-Hill Book Co., 1993

Zhou, Lifu, *Fabrication of Quantum Well Detector Array for Thermal Imaging,* Chapter 5, Master's Thesis, National University of Singapore, 2001.

INITIAL DISTRIBUTION LIST

1. Defense Technical Information Center
    Ft. Belvoir, VA

2. Dudley Knox Library
    Naval Postgraduate School
    Monterey, CA

3. Chairman (Code PH)
    Department of Physics
    Naval Postgraduate School
    Monterey, CA

4. Gamani Karunasiri
    Naval Postgraduate School
    Monterey, CA

5. James Luscombe
    Naval Postgraduate School
    Monterey, CA

6. LT Michael Touse
    United States Navy
    Norfolk, VA